



# Interface Microstructure and Tribological Behaviors of Copper Matrix Composites with High Graphite Content Prepared by Short-Process Reduction and Vacuum Hot Pressing

TAO ZHOU,<sup>1</sup> JIE DAI,<sup>1</sup> ZHU XIAO ,<sup>1,2,5</sup> WEN-TING QIU,<sup>1</sup> QIAN LEI,<sup>3</sup> XINWEI LIU,<sup>4</sup> LIUXIN QIN,<sup>1</sup> and MUZHI MA<sup>1</sup>

1.—School of Materials Science and Engineering, Central South University, Changsha 410083, China. 2.—Key Laboratory of Non-ferrous Metal Materials Science and Engineering, Ministry of Education, Changsha 410083, China. 3.—State Key Laboratory for Powder Metallurgy, Central South University, Changsha 410083, China. 4.—Zhejiang Tianning Alloy Material Co., Ltd, Jinhua 321002, China. 5.—e-mail: xiaozhumse@163.com

Combining short-process reduction and vacuum hot pressing, copper matrix composites with the graphite volume fraction of 55% and 70% were prepared by cuprous oxide and spherical graphite (Cu<sub>2</sub>O-Gr composites). Transmission electron microscopic (TEM) results show that some graphite particles in Cu<sub>2</sub>O-Gr composites change from spherical to finer flocculent or acicular shape, and the interface between the matrix and graphite is partially coherent. The reaction enhances interface bonding and modifies the interface morphology of graphite, leading to the good mechanical performance of the composites. Compared with the Cu-Gr composites prepared by conventional hot pressing, the Cu<sub>2</sub>O-Gr composites present higher density and strength and lower friction coefficients and wear rates. In the current-carrying friction experiments, the wear rate of the Cu<sub>2</sub>O-55Gr is nearly 25% lower than that of the Cu-55Gr. The short-process reduction contributes to better self-lubricating behaviors of the Cu<sub>2</sub>O-Gr composites, reducing the adhesive wear and abrasion wear.

## INTRODUCTION

Copper-graphite composites have been widely used as sliding components in the engineering field, e.g., brushes, electrodes, alternators and carbon slides of pantographs, because of the combination of high electrical conductivity, high thermal conductivity and fine self-lubricating properties.<sup>1–3</sup> The optimum self-lubricating and electrical contact properties of composites can be controlled by the composition of copper-graphite.<sup>4</sup> However, to obtain low friction coefficients, copper-graphite composite usually contains a high graphite content, leading to the decrease of the mechanical properties (e.g., hardness and fracture strength) of the composites.<sup>5</sup> It is essential to improve the mechanical and electrical properties to prolong the service life of

the composite products. Therefore, the improvement the friction and mechanical properties of the copper-graphite composite is still a research topic of great interest for copper-graphite composite.<sup>6,7</sup>

The preparation method plays a key role in the mechanical and tribological properties of copper matrix composites.<sup>8–10</sup> For conventional Cu-graphite composite, neither wetting nor chemical reaction could occur between copper and graphite even at a high temperature above the melting point of copper, weakening the interface bonding and decreasing the properties of Cu-graphite composites.<sup>11</sup> It was reported that Cr, Ag and Ti coatings on graphite particles could improve the wettability between the copper matrix and graphite, which enhanced the bonding strength of the interface and improved the mechanical properties of Cu-graphite composites.<sup>12–14</sup> The interface microstructure results showed that the diffusion layer or carbide formed at the interface by adding Si, W, Mo and

other elements into the copper matrix; however, little work has been done on the friction properties of the composite.<sup>15–17</sup> Some solid lubricants, such as MoS<sub>2</sub>, WS<sub>2</sub>, graphene and carbon nanotubes, can also strengthen the interface bonding of Cu matrix composites.<sup>18–20</sup> Nevertheless, these methods are quite complicated as well as expensive and use many chemical reagents.

The volume fraction, size, morphology and distribution of graphite particles are important for the mechanical properties and tribological behaviors of Cu-graphite composites.<sup>21</sup> Liu et al.<sup>22</sup> reported that the flexural and compressive strength increased with the decrease of graphite particle size. Kováčik et al.<sup>23</sup> suggested that the fine graphite powder could make the distribution of graphite particles very uniform, leading to the formation of a continuous self-lubricating layer on the contact surface during the wearing test. Nano-sized graphite could increase the wear resistance and decrease the friction coefficients of the Cu-graphite composites.<sup>24</sup> The Cu-graphite composites with higher hardness and strength often had lower wear rates,<sup>25</sup> and the wear mechanisms were usually adhesive, abrasive and electrical erosion wear, etc.<sup>4</sup>

Recently, the author found that the Cu-graphite composites could be satisfactorily produced by in situ reaction ( $2\text{Cu}_2\text{O}(\text{s}) + \text{C}(\text{graphite}) \rightarrow 4\text{Cu}(\text{s}) + \text{CO}_2(\text{g})$ ) using cuprous oxide and graphite.<sup>25,26</sup> This method to produce high-quality Cu-graphite composites is inexpensive, efficient and simple. In this article, a modified short process of in situ oxidation-reduction reaction method was used to produce Cu<sub>2</sub>O-Gr composites with high graphite contents. As a comparison, Cu-Gr composites using copper powders and graphite powders as the raw materials were also produced. The interface microstructure and tribological behaviors of the composites were investigated in detail.

## MATERIALS AND EXPERIMENTAL METHODS

### Composites Preparation Process

The raw materials used in the experiment included spherical graphite powder (99.95% purity with average particle size of 19 μm and density of 2.25 g/cm<sup>3</sup>, supplied by Qingdao Tengshengda Co., Ltd.), cuprous oxide powder (99% purity with particle size of 5 μm and density of 6.0 g/cm<sup>3</sup>, supplied by Aladdin Co., Ltd.) and electrolytic copper powder (99.9% purity with particle size of 5 μm and density of 8.9 g/cm<sup>3</sup>, supplied by Grinn Advanced Materials Co., Ltd.).

The spherical graphite was first pre-treated by undergoing the following steps:

(1) Removing the oil and broken graphite from the surface of the graphite powder. Solution formulation: NaOH (100 g/L), Na<sub>2</sub>CO<sub>3</sub> (25 g/L) and Na<sub>3</sub>PO<sub>4</sub> (25 g/L). The graphite powder was mixed into the solution and kept above 95°C for 1 h to remove the

organic matter adsorbed on the surface of graphite powders.

(2) Coarsening the graphite powder. Solution formulation: HNO<sub>3</sub> (65%, 200 ml/L). The graphite powder was mixed into the solution and kept above 95°C for 1 h and then dried in oven at 50°C for 2 h. The purpose was to form coronal pits on the graphite surface, increase the specific surface area and surface energy and enhance the anchoring effect between the interface and the matrix. Figure 1 shows that the spherical graphite is smoother after pretreatment, showing that less broken graphite was left.

The amount of the reaction between the cuprous oxide and graphite should be considered when weighing the raw materials. The powders were mixed in V mixer for 2 h, and 2–3 vol% alcohol was added. To shorten the process flow, a modified in situ oxidation-reduction reaction and vacuum hot-pressing method was used to produce samples. First, the mixed powders were put into a copper pipe with a thickness of 0.8 mm directly without cold pressing. The wrapping of copper pipe can avoid the reaction between cuprous oxide and graphite mold during hot pressing. The powder mixtures were then hot-pressed in a vacuum of 10<sup>-2</sup> Pa. The hot-pressing process is shown in Fig. 2. Temperature rose from room temperature to 850°C in 1 h, and 20 MPa pressure was applied on the mixture sample. Then, keeping temperature at 850°C for 3 h to complete the reaction, the 20 MPa pressure could ensure the tight contact between the Cu<sub>2</sub>O and graphite powders and the smooth evacuation of the generated CO<sub>2</sub> from the mold. The pressure of 50 MPa and temperature of 950°C for 1.5 h were used to make the composite fully sintered and compact. The Cu-Gr composites were prepared under the same process conditions.

### Experimental Details

Scanning electron microscope (SEM) with EDS (Oxford XMAX20), x-ray diffraction (DMAX-2500) and transmission electron microscope (TEM TECNAI G2 F20) were used to analyze the interface microstructure and composition of the composites. The densities of the composites were measured according to the Archimedes principle. The Vickers hardness of the composites was measured by HV-3300 Vickers hardness tester, with a test force of 200 gf. Compressive strength was measured at the speed of 0.5 mm/min on an Instron universal testing machine (3369-Model), and the sample was Φ8 mm × 8 mm cylinder.

The friction and wear properties of the composites in air (relative humidity: 50%, temperature: 25°C) were tested on a CSM friction and wear tester, with sliding speed of 2 m/s and sliding distance of 1000 m. The normal load was 2 N, 6 N and 10 N and the current was 0 A, 0.5 A and 1 A, respectively. The disc was made of pure copper, with a hardness of

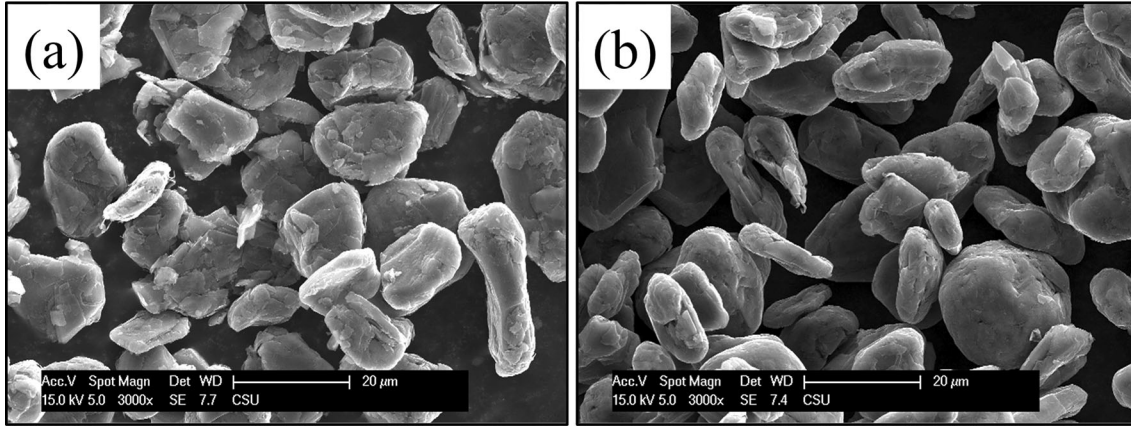


Fig. 1. (a) Spherical graphite; (b) spherical graphite after pretreatment.

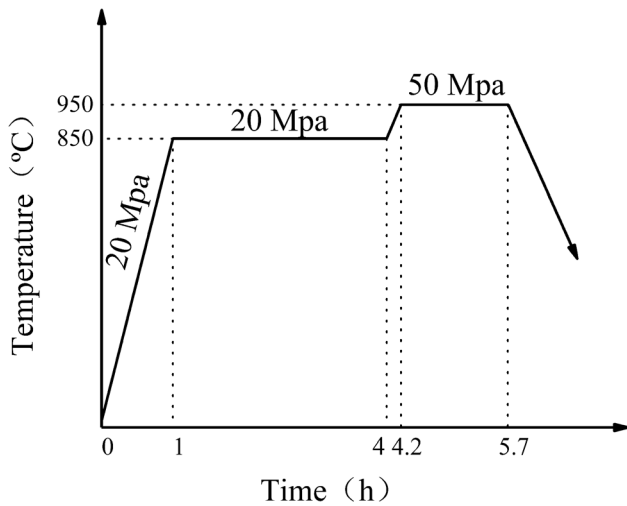


Fig. 2. Technological process of vacuum hot pressing.

100 HV. The specimen was a semicircular block, with a thickness of 3 mm and diameter of 10 mm. The wear mass loss was measured by an analytical balance (0.0001 g precision, TE214S-Model). Three specimens were tested for each composite, and the average values of the friction coefficient and wear mass loss were taken. SEM observations were carried out for viewing the worn surfaces of composites.

The friction coefficient of composite was calculated by the following formula:

$$\mu = \frac{P - P_0}{Fv} \quad (1)$$

where  $\mu$  is the friction coefficient,  $P$  is the power of the electric motor when composites contact the disc (unit: W),  $P_0$  is the power of the electric motor when composites do not contact with the disc (W),  $F$  is the normal load applied to the specimen (N), and  $v$  is the sliding speed (m/s).

Wear rate was calculated by the following formula:

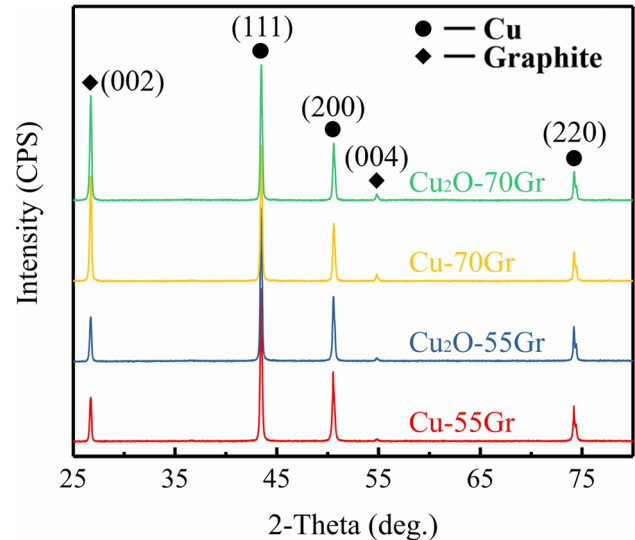


Fig. 3. XRD patterns of the Cu-Gr and  $\text{Cu}_2\text{O}$ -Gr composites.

$$w = \frac{V}{Fl} \quad (2)$$

where  $w$  is the wear rate,  $V$  is the worn volume of the specimen ( $\text{mm}^3$ ), which can be calculated with wear mass loss and the densities of the specimens,  $F$  is the normal load applied (N), and  $l$  is the sliding distance of specimen (m).

## RESULTS

### XRD Analysis of the Composites

The XRD patterns of the  $\text{Cu}_2\text{O}$ -Gr and Cu-Gr composites with 55 and 70 vol% graphite (samples were expressed as  $\text{Cu}_2\text{O}$ -55Gr,  $\text{Cu}_2\text{O}$ -70Gr, Cu-55Gr, Cu-70Gr in this paper) are shown in Fig. 3. The patterns of the four composites are very similar, and only graphite and Cu can be detected in Fig. 3. There was no oxidation during the hot-pressing

process, and  $\text{Cu}_2\text{O}$  fully reacted and transformed into Cu, consistent with the results in Ref.<sup>25</sup>

### Interface Microstructure of the Cu-Gr and $\text{Cu}_2\text{O}$ -Gr Composites

Figure 4 shows the interface microstructure of the Cu-Gr and  $\text{Cu}_2\text{O}$ -Gr composites. For Cu-Gr samples, some graphite particles fall off during polishing, forming holes and cracks at the interface (as shown in the red box of Fig. 4a-c), and graphite particles agglomerate obviously in the Cu-55Gr and Cu-70Gr composites. For  $\text{Cu}_2\text{O}$ -Gr composites shown in Fig. 4d-f, there are basically no cracks and pits at the interface between graphite particles and copper matrix, and graphite particles are evenly distributed in the  $\text{Cu}_2\text{O}$ -55Gr and  $\text{Cu}_2\text{O}$ -70Gr composites. The sizes and morphology of some graphite particles change significantly from near spherical to irregular wire shape because of the reaction between the  $\text{Cu}_2\text{O}$  and graphite at the interface, especially in the  $\text{Cu}_2\text{O}$ -55Gr (as shown in the yellow box). It is worth noting in Fig. 4f that some Cu generated by  $\text{Cu}_2\text{O}$  exists inside graphite particles (shown by red arrow).

The element line distribution in the interface region was studied to better understand the effect of the reaction on the composition of composites. In Fig. 4g, the distribution of Cu and C elements is clearly observed in the Cu-70Gr composite. In Fig. 4h, the abnormal C peak appears in the  $\text{Cu}_2\text{O}$ -70Gr composite (marked with the arrow in Fig. 4h), while no obvious graphite particles are found.

According to the SEM images, the Cu-55Gr and Cu-70Gr composites present similar results, and there is also no fundamental microstructural difference between the  $\text{Cu}_2\text{O}$ -55Gr and  $\text{Cu}_2\text{O}$ -70Gr samples. Therefore, Cu-55Gr and  $\text{Cu}_2\text{O}$ -55Gr were chose for further TEM study, as shown in Fig. 5. The graphite in the Cu-55Gr presents stick and lamellar shapes (Fig. 5a, b). The obvious gap (circled in Fig. 5a) at the interface indicates that graphite is not tightly bonded with copper matrix. Figure 5c shows that the graphite size of the  $\text{Cu}_2\text{O}$ -55Gr decreases greatly after the reaction and finally forms flocculent and acicular shapes. The EDS analysis of region 2 in Fig. 5d shows that some residual graphite particles of 5–30 nm size are

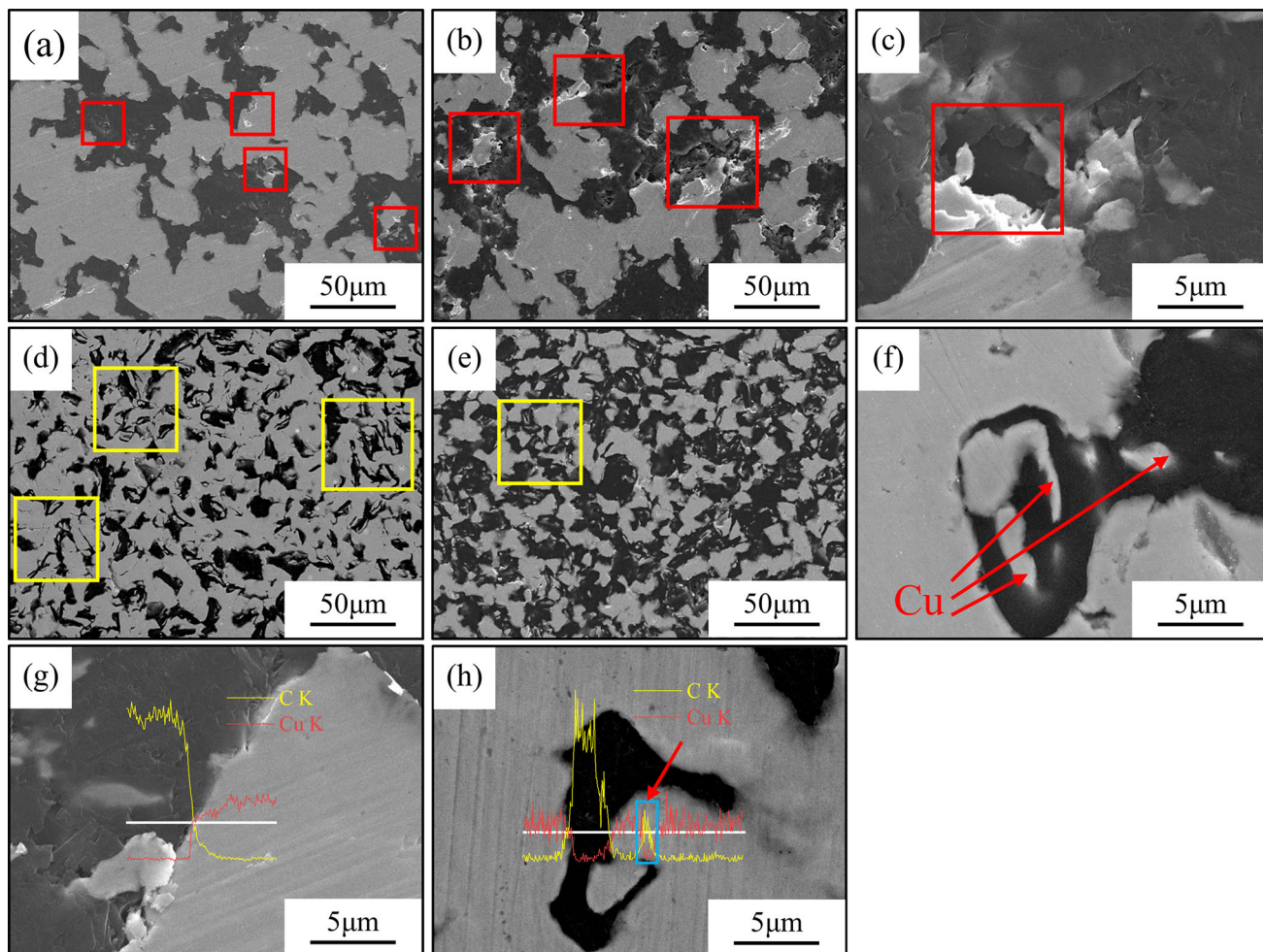


Fig. 4. (a) Cu-55Gr; (b, c) Cu-70Gr; (d)  $\text{Cu}_2\text{O}$ -55Gr; (e, f)  $\text{Cu}_2\text{O}$ -70Gr; (g) line scanning of the Cu-70Gr; (h) line scanning of the  $\text{Cu}_2\text{O}$ -70Gr.

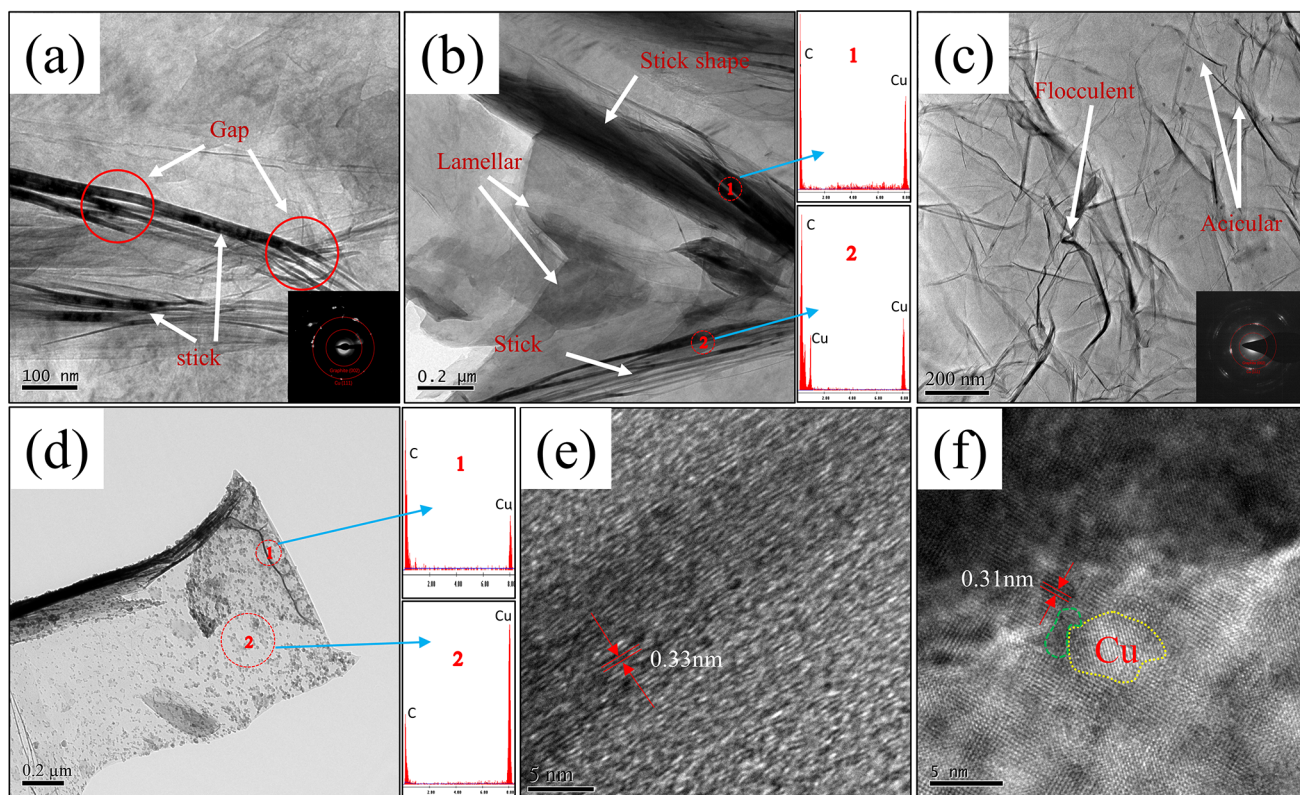


Fig. 5. TEM images and EDS analysis of the Cu-55Gr and  $\text{Cu}_2\text{O}$ -55Gr composites: (a, b) Cu-55Gr; (c, d)  $\text{Cu}_2\text{O}$ -55Gr; (e) high-resolution image of graphite; (f) high-resolution image of the  $\text{Cu}_2\text{O}$ -55Gr.

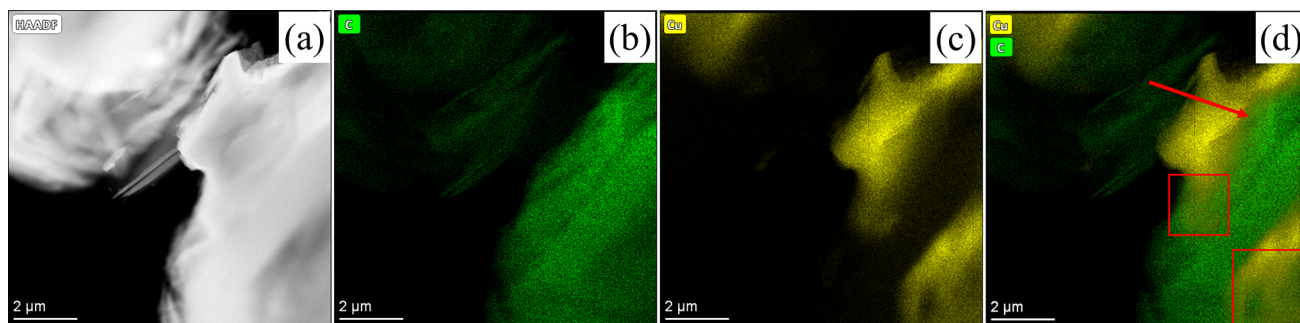


Fig. 6. HAADF image (a) and EDS elemental mapping of the  $\text{Cu}_2\text{O}$ -55Gr: (b) C; (c) Cu; (d) Cu and C.

uniformly distributed in the copper matrix after the reaction. A typical high-resolution image of graphite in the  $\text{Cu}_2\text{O}$ -55Gr composite is shown in Fig. 5e. The interplanar spacing of the graphite is about 0.33 nm, indicating that no obvious reaction occurred in this part. Figure 5f indicates that the interface between the Cu and graphite is partially coherent after the reaction (circled in yellow).

The  $\text{Cu}_2\text{O}$ -55Gr composite was analyzed using high-angle annular dark-field (HAADF) STEM coupled with EDS, as shown in Fig. 6. EDX maps exhibit an overlay of C and Cu elements (Fig. 6d), and the boundary between the Cu and C segments is indistinct (shown by the red box). Moreover, there

is a transition region at the interface of Cu and graphite (shown by the red arrow).

### Physical and Mechanical Properties of the Composites

The physical and mechanical properties of the composites are summarized in Table I. Compared with the Cu-Gr composites, the  $\text{Cu}_2\text{O}$ -Gr composites show better mechanical properties. The densities of  $\text{Cu}_2\text{O}$ -Gr are about 4% higher than those of Cu-Gr, and the compression strength of  $\text{Cu}_2\text{O}$ -Gr is about 25-40% higher than that of Cu-Gr. The electrical conductivities of Cu-Gr and  $\text{Cu}_2\text{O}$ -Gr are approximately equal. The evolution of properties of the Cu-Gr and  $\text{Cu}_2\text{O}$ -Gr composites in this study is close to

those reported in Ref.<sup>25</sup> suggesting that the shortened process is also suitable for producing Cu<sub>2</sub>O-Gr composites with high strength.

The compressive fracture morphology of the composites and compressive curve of the composites are shown in Fig. 7. In Fig. 7a, b, the fracture surface of the Cu<sub>2</sub>O-70Gr composite is rougher than that of the Cu-70Gr composite. In Fig. 7c, all samples show brittle fracture. The in situ reaction clearly improved the compressive strength and reduced the ductility of the composites. In addition, all samples fractured at an inclined angle of 45°, suggesting that the brittle fracture occurred in the composites.

### Tribological Behaviors

The average friction coefficients of the composites under different load values are listed in Table II. Overall, the friction coefficients of the Cu<sub>2</sub>O-Gr composites are lower than those of the Cu-Gr composites at any given load value and volume fraction of graphite. With the increase of load values from 2 N to 6 N, the friction coefficients of the composites show an obvious downward trend. With the load increasing from 6 N to 10 N, the friction coefficient of the Cu-70Gr composite increases obviously, while the others change slightly.

The relationship between the friction coefficients and the sliding distance of the composites under different load values is shown in Fig. 8. With the increase of sliding distance, the friction coefficients fluctuate greatly first and then tend to be stable at large sliding distances. The Cu-70Gr and the Cu<sub>2</sub>O-70Gr composites present shorter instability stage

and smoother curve compared to the Cu-55Gr and Cu<sub>2</sub>O-55Gr composites.

The variation of wear rates of composites with the load values is shown in Fig. 9. At any given graphite content, the wear rates of the Cu<sub>2</sub>O-Gr composites are lower than those of the Cu-Gr composites. Notably, with the increase of load values from 2 N to 10 N, the wear rates of the Cu-55Gr, Cu<sub>2</sub>O-55Gr and Cu<sub>2</sub>O-70Gr composites first decrease and then increase, while the wear rates of the Cu-70Gr composite keep increasing with the sliding distance.

SEM images of the composites after friction are shown in Fig. 10. Compared to the Cu-Gr (Fig. 10a-c), the friction surface of the Cu<sub>2</sub>O-Gr is smoother (Fig. 10d-f). The wear modes of the Cu-Gr composites are appreciable adhesive and abrasive wear. There are obvious cracks (circled in red) and grooves (marked in yellow) on the surface, and much wear debris is left (circled in blue). The wear mode of the Cu<sub>2</sub>O-Gr composites is micro-plowing, with little wear debris and few grooves left.

### Current-Carrying Tribological Behaviors

The Cu<sub>2</sub>O-55Gr presented a much better self-lubrication property than the Cu-55Gr at the load of 2 N (Table II), and these two samples were used to further study the current-carrying tribological behaviors of the composites at 2 N.

The average friction coefficients of the composites at different current values are listed in Table III. Figure 11a shows the relationship between the friction coefficients and sliding distance of the Cu-55Gr and Cu<sub>2</sub>O-55Gr composites at different currents. Figure 11b gives the variations of wear rates

**Table I. Physical and mechanical properties of the composites**

Composites	Density (g/cm <sup>3</sup> )	Hardness (HV)	Compression strength (MPa)	Electrical conductivity (%IACS)
Cu-55Gr	5.003 ± 0.01	21.7 ± 0.80	100.3 ± 1.97	24.6 ± 0.41
Cu <sub>2</sub> O-55Gr	5.183 ± 0.01	32.8 ± 0.46	141.4 ± 0.04	24.9 ± 0.26
Cu-70Gr	4.014 ± 0.02	14.9 ± 0.55	53.8 ± 2.65	8.0 ± 0.19
Cu <sub>2</sub> O-70Gr	4.166 ± 0.01	20.4 ± 0.75	67.4 ± 2.04	8.2 ± 0.33

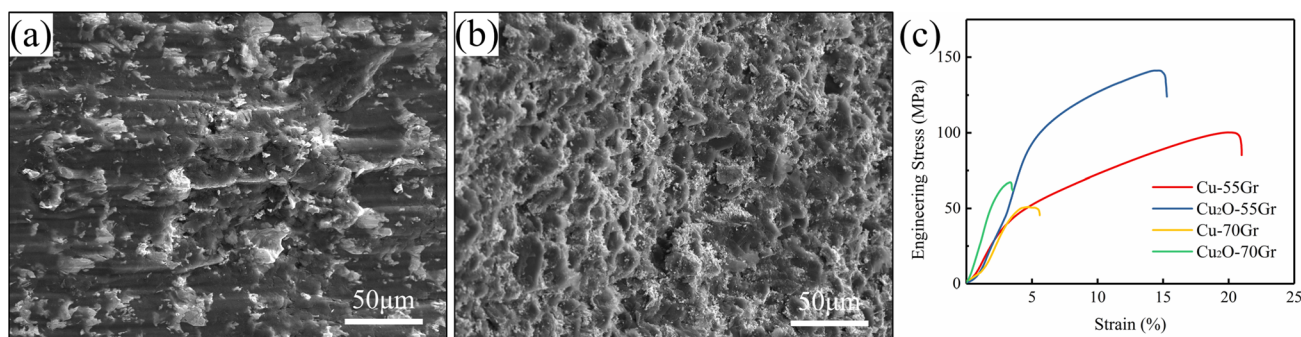


Fig. 7. (a) Fracture of Cu-70Gr; (b) fracture of Cu<sub>2</sub>O-70Gr; (c) compressive curve.

**Table II. Average friction coefficients of composites at different load values**

Load	2 N	6 N	10 N
Cu-55Gr	$0.328 \pm 0.004$	$0.268 \pm 0.013$	$0.257 \pm 0.018$
Cu <sub>2</sub> O-55Gr	$0.267 \pm 0.003$	$0.241 \pm 0.010$	$0.255 \pm 0.004$
Cu-70Gr	$0.259 \pm 0.002$	$0.185 \pm 0.003$	$0.211 \pm 0.006$
Cu <sub>2</sub> O-70Gr	$0.277 \pm 0.002$	$0.182 \pm 0.005$	$0.185 \pm 0.003$

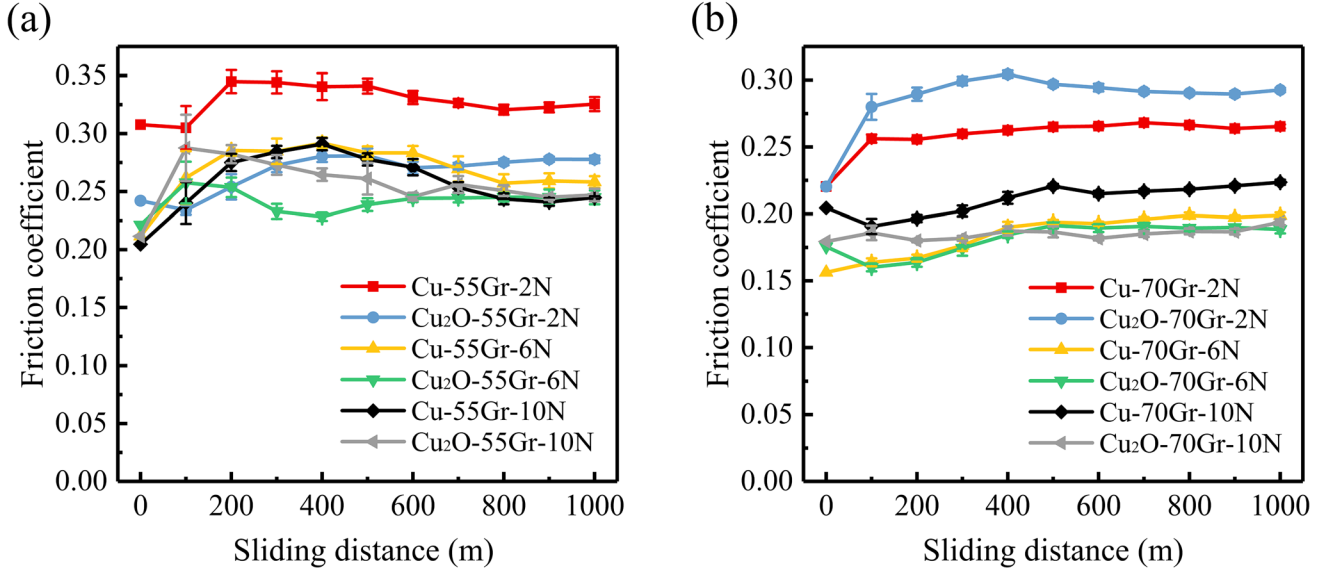
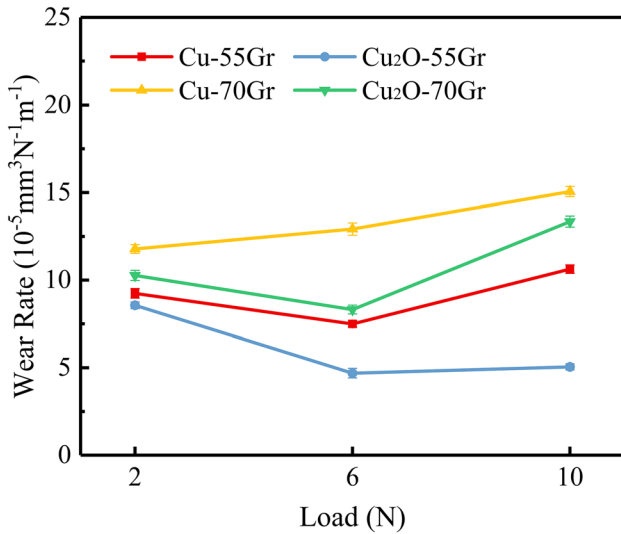
Fig. 8. Friction coefficients of the composites: (a) Cu-55Gr and Cu<sub>2</sub>O-55Gr; (b) Cu-70Gr and Cu<sub>2</sub>O-70Gr.

Fig. 9. Wear rates of the composites.

with current of the Cu-55Gr and Cu<sub>2</sub>O-55Gr composites. The Cu<sub>2</sub>O-55Gr composite presents a lower friction coefficient than the Cu-55Gr composite, and the wear rate of the Cu<sub>2</sub>O-55Gr composite is about 25% lower than that of the Cu-55Gr composite, suggesting that the Cu<sub>2</sub>O-55Gr has a better self-lubrication property in current-carrying friction. In addition, with the increase of the current, the

friction coefficients decrease but the wear rates increase.

SEM images of the Cu-55Gr and Cu<sub>2</sub>O-55Gr after current-carrying friction are shown in Fig. 12, and arc ablation occurs in both samples (circled in blue). Compared to the Cu-55Gr sample, the wear surface of the Cu<sub>2</sub>O-55Gr sample is smoother, with fewer cracks left (circled in red). Figures 10a and 12a indicate that the decrease of the cracks (circled in red) could be attributed to the presence of electric current. Instantaneous high temperature resulting from the current helps graphite to fall off from the matrix, improving the self-lubricant effect.

## DISCUSSION

### Advantages of the Short-Process Reduction

Interface microstructure of the Cu<sub>2</sub>O-Gr composites (Figs. 4–6) confirms that the reaction of Cu<sub>2</sub>O with graphite modifies the interface of Cu (products of Cu<sub>2</sub>O) and graphite at atomic scale.<sup>25</sup> The sizes and morphology of graphite particles change greatly owing to the reaction, while little change happens during conventional hot pressing, as shown in Fig. 13. The outer graphite involved in the reaction is not completely consumed, and then the remaining tiny graphite particles disperse randomly in the copper matrix (Fig. 5d), finally forming an abnormal

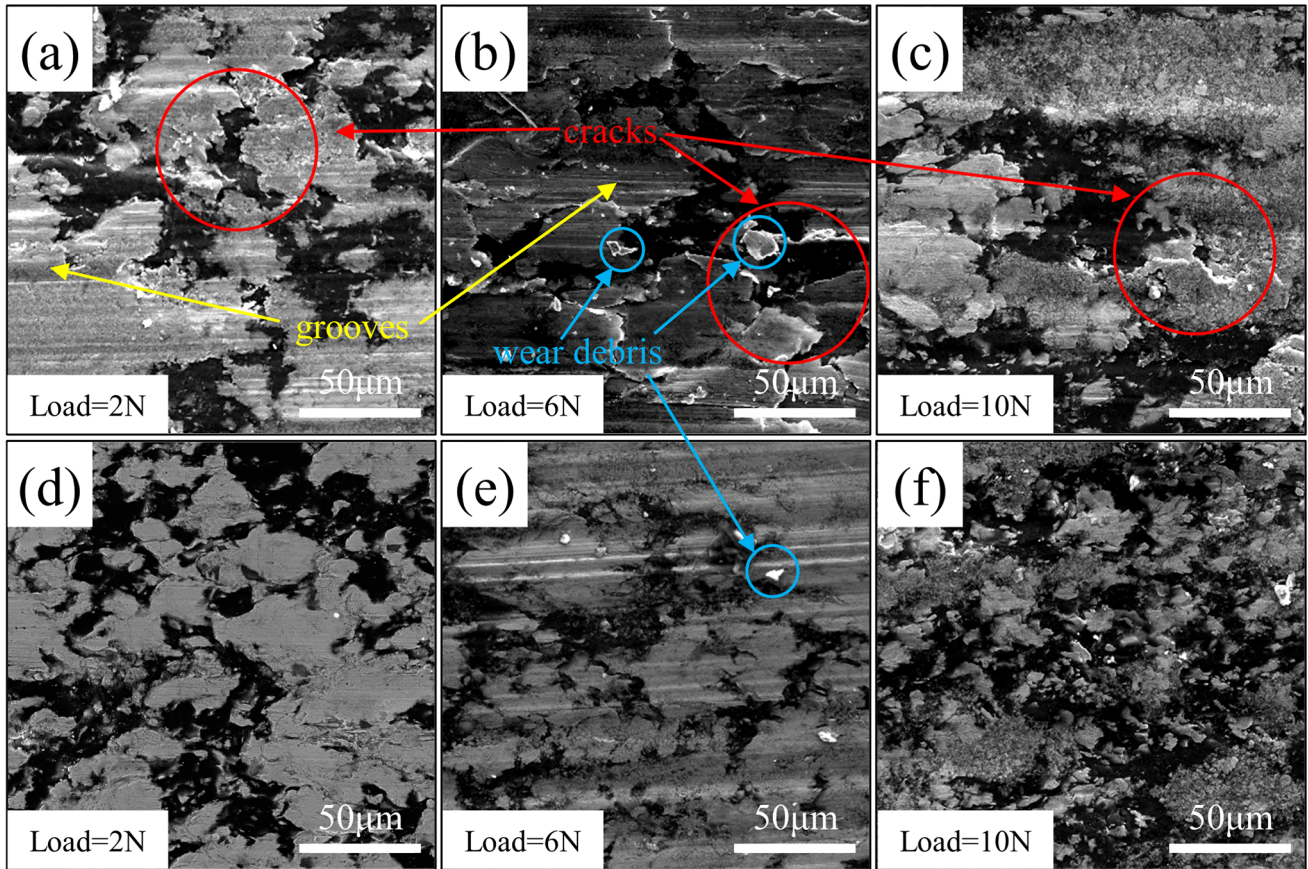


Fig. 10. Images of the composites after friction: (a, b) Cu-55Gr; (c) Cu-70Gr; (d, e) Cu<sub>2</sub>O-55Gr; (f) Cu<sub>2</sub>O-70Gr.

**Table III. Average friction coefficients of composites at different current values, at the load of 2 N**

Current	0 A	0.5 A	1 A
Cu-55Gr	0.328 ± 0.004	0.278 ± 0.006	0.267 ± 0.008
Cu <sub>2</sub> O-55Gr	0.267 ± 0.003	0.227 ± 0.008	0.210 ± 0.011

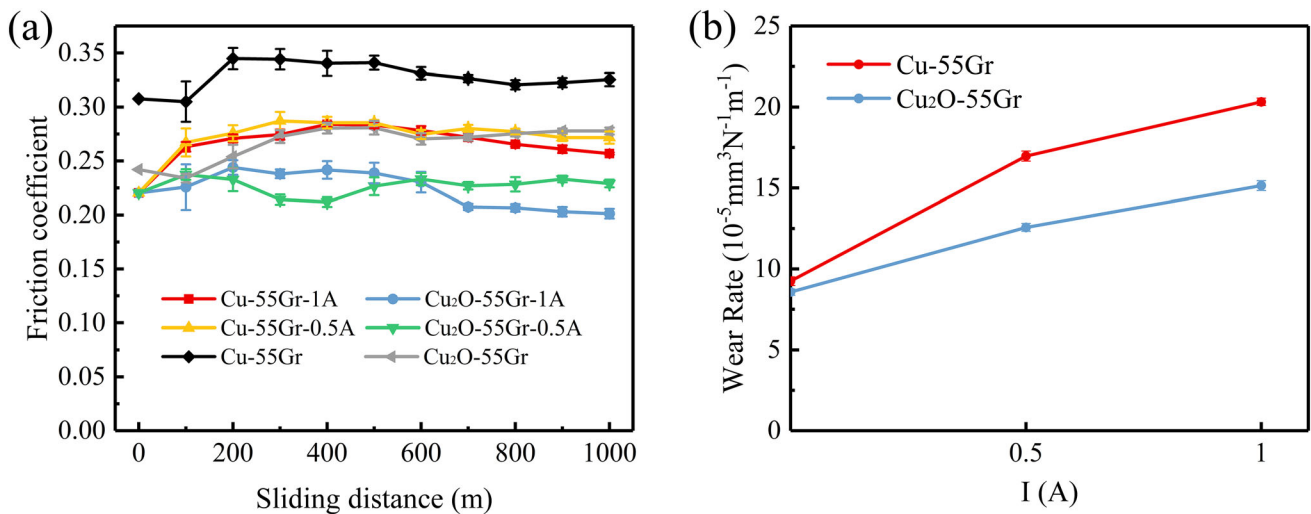


Fig. 11. (a) Cu-55Gr and Cu<sub>2</sub>O-55Gr under different currents at 2 N. (b) Wear rates of the Cu-55Gr and Cu<sub>2</sub>O-55Gr under different currents at 2 N.



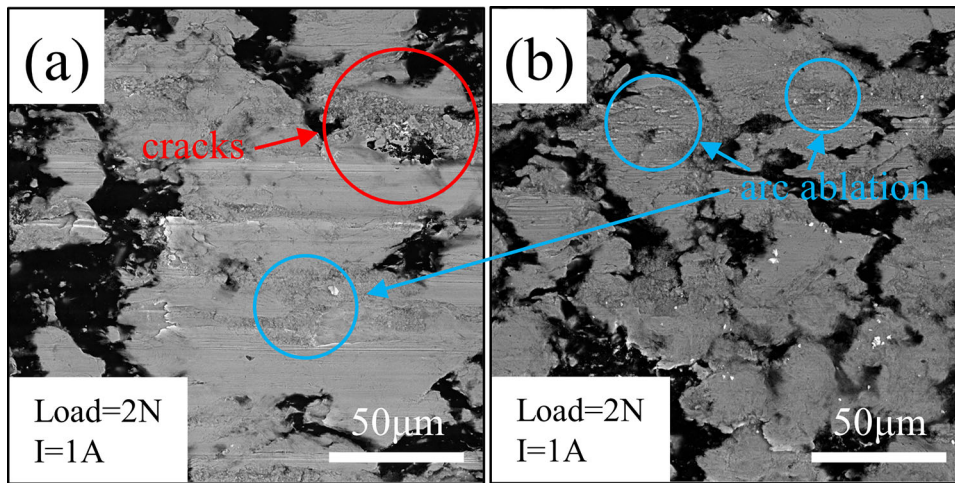


Fig. 12. SEM images of the Cu-55Gr and  $\text{Cu}_2\text{O}$ -55Gr: (a) Cu-55Gr,  $I = 1\text{A}$ ; (b)  $\text{Cu}_2\text{O}$ -55Gr,  $I = 1\text{A}$ .

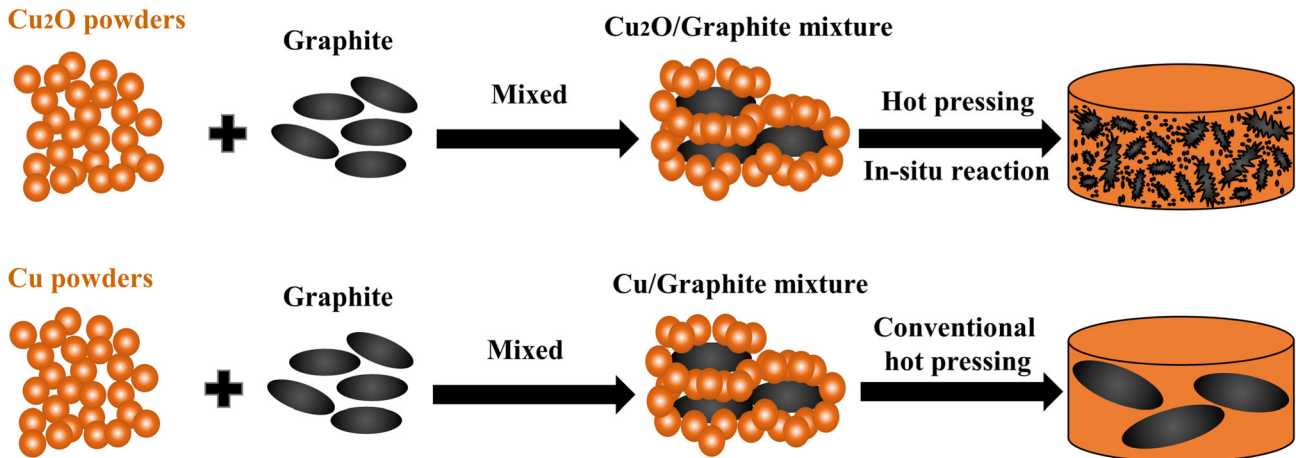


Fig. 13. Sizes and morphology changes of raw materials during hot pressing.

C peak, shown in Fig. 4h. Although the wettability between the graphite and copper is very poor,<sup>2,27,28</sup> the copper that forms by the reaction can “penetrate” into the graphite particles (Fig. 4f), reducing the agglomeration of graphite and enhancing the good interface bonding.

Layer reduction,<sup>29</sup> refinement,<sup>30,31</sup> modified interface<sup>14,32</sup> and irregular shape<sup>33</sup> of graphite phase in Cu matrix are helpful for improvement of the mechanical properties. Uniform distribution<sup>34</sup> of graphite promotes a continuous three-dimensional structure of copper, reducing the trend of fracture. In this study, the reaction contributes to finer and irregularly shaped graphite, promoting the homogeneous dispersion of graphite and enhancing the interface bonding between Cu and graphite, leading to the increase of the mechanical properties of the  $\text{Cu}_2\text{O}$ -Gr composites.

The smooth fracture surface (Fig. 7b) should be attributed to the agglomerated graphite particles of the Cu-70Gr composite, increasing the tendency of separation and slipping.<sup>2,35</sup> The tiny irregular graphite particles and good interface bonding in

the  $\text{Cu}_2\text{O}$ -Gr composite decrease the tendency of crack initiation and propagation between Cu and graphite,<sup>14</sup> leading to a rough fracture surface.

### Friction and Wear Mechanism

The lubrication film on the surface is not completely formed at the beginning of wearing, and the contact mode between the composites and the friction disc is mainly metal-metal contact.<sup>36</sup> This contact mode is prone to bite and adhesion, and thus unstable friction occurs. With increasing sliding distance, the graphite particles released on the worn surface can promote the formation of a thin lubricating film on the contact surface, which makes the contacting mode gradually change to metal-lubrication film-metal contact.<sup>21</sup> At this point, the friction mainly occurs in the solid lubrication film, reducing the overall friction coefficient and wear rate.<sup>37</sup> The friction coefficient tends to be stable when the formation and wear rates of the lubrication film reach a dynamic balance.<sup>38</sup>

The composites present adhesive and abrasive wear in the friction experiment. The fine and evenly distributed graphite particles and better interface bonding in the Cu<sub>2</sub>O-Gr composites promote the formation of continuous lubrication film, significantly reducing the adhesive wear.<sup>21,24,39,40</sup> At a relatively low load (2 N), the graphite particles worn off from the surface of the composites are too few to form a continuous lubricating film, leading to a high friction coefficient and wear rate. Increase of the load (6 N, 10 N) promotes the separation of the graphite particles from the matrix, reducing the friction coefficient of the composite. However, excessive load (10 N) may result in severe plastic deformation on the friction surface,<sup>41</sup> which accelerates the wear rate and results in the deterioration of the lubrication effect (Table II, Cu-70Gr), especially when the mechanical properties of the material are poor. In addition, the friction temperature increases with the increase of load during friction, which may cause local oxidation and decrease of mechanical properties.<sup>42</sup>

With the increase of current, the friction coefficients of the Cu<sub>2</sub>O-55Gr and Cu<sub>2</sub>O-55Gr composites decrease, while the corresponding wear rates increase. For the same material, when the friction speed is constant, the friction heat generated by the friction surface is roughly equal, and the current increases the resistance heat of the friction surface ( $Q = I^2R$ ). Accumulation of resistance heat and friction heat leads to the serious oxidation of graphite and destruction of the graphite lubricating layer, enhancing the roughness of the friction surface.<sup>18</sup> The rough friction surface promotes the generation of arc, and arc ablation becomes serious when the current is large.<sup>43</sup> The instantaneous high temperature brought by the arc will melt the material surface to form a liquid metal film, reducing the friction coefficient of the composite. Meanwhile, copper tends to be oxidized at the high temperature caused by the arc, resulting in the increase of the wear rate.<sup>36,42</sup> The arc weakens the surface matrix strength,<sup>24</sup> leading to the increase of the wear rates. In the current-carrying friction experiment, the main wear mechanisms of the composites are adhesive wear and arc ablation.

### Wear Coefficient

The friction force in a friction test could be caused by the combination of adhesion and abrasion wear (grooves left).<sup>44,45</sup> If the adhesive part of the friction does not interact with the groove part, the friction force  $F_f$  can be written as:

$$F_f = F_p + F_a \quad (3)$$

where  $F_p$  is the plowing force caused by the plastic deformation of the composites, and  $F_a$  is the adhesion force between the composites and friction disc. Therefore, the friction coefficient ( $\mu$ ) of the composites can be calculated by:

$$\mu = \frac{F_f}{F_n} = \frac{F_p}{F_n} + \frac{F_a}{F_n} = \mu_p + \mu_a \quad (4)$$

where  $F_n$  is the normal force applied to the sample,  $\mu_p$  is the friction coefficient caused by plowing, and  $\mu_a$  is the friction coefficient caused by adhesion. According to Fig. 10, an unsatisfactory friction effect of the Cu-Gr composites resulted from weak interface bonding and agglomeration of graphite particles, leading to much more adhesive wear.

Based the Archard abrasive wear model,<sup>46</sup> the total wear volume ( $V$ ) of the composites during the friction process can be written as:

$$V = k \frac{F}{H} D \quad (5)$$

where  $H$  is the hardness of the material (N/mm<sup>2</sup>),  $k$  is the wear coefficient,  $D$  is the sliding distance, and  $F$  is the load value on the composites. According to Eqs. 5, 6 obtained:

$$k = \frac{H}{FD} V \quad (6)$$

The  $\frac{V(\text{Cu}_2\text{O-Gr})}{V(\text{Cu-Gr})}$  can be calculated by Fig. 9 and Eq. 2, and the  $\frac{H(\text{Cu}_2\text{O-Gr})}{H(\text{Cu-Gr})}$  can be measured in the experiments; thus, the  $\frac{k(\text{Cu}_2\text{O-Gr})}{k(\text{Cu-Gr})}$  at the same condition ( $F$  and  $D$ ) can be calculated:

$$k_p = \frac{k(\text{Cu}_2\text{O-Gr})}{k(\text{Cu-Gr})} = \frac{V(\text{Cu}_2\text{O-Gr})}{V(\text{Cu-Gr})} \cdot \frac{H(\text{Cu}_2\text{O-Gr})}{H(\text{Cu-Gr})} \quad (7)$$

The  $\frac{k(\text{Cu}_2\text{O-Gr})}{k(\text{Cu-Gr})}$  of the composites at different loads is summarized in Table IV. At relatively low load (2 N), extrusion of graphite particles from the Cu<sub>2</sub>O-Gr matrix (the Cu<sub>2</sub>O-Gr presents better interface bonding and mechanical properties) to form lubricating film is more difficult, weakening the lubrication effect of the Cu<sub>2</sub>O-Gr and leading to a higher  $k_p$ . At relatively high load (10 N), the higher  $k_p$  of the Cu<sub>2</sub>O-70Gr can be attributed to the severe plastic deformation, reducing the mechanical properties and wear resistance.<sup>41</sup> Under the other conditions, the Cu<sub>2</sub>O-Gr composite shows a smaller wear coefficient, indicating more efficient lubrication.<sup>47</sup>

### CONCLUSIONS

1. Cu-graphite composites were successfully produced by short-process reduction and vacuum hot-pressing method. The interface bonding between Cu and graphite in the Cu<sub>2</sub>O-Gr composites is better than that of the Cu-Gr composites. Some graphite particles in Cu<sub>2</sub>O-Gr composites change from spherical to finer flocculent or acicular shape because of the in situ reaction, and the interface between the matrix and graphite is partially coherent.

**Table IV. The  $\frac{k(\text{Cu}_2\text{O}-\text{Gr})}{k(\text{Cu}-\text{Gr})}$  of the composites at different loads**

$k_p$	2 N	6 N	10 N
$\frac{k(\text{Cu}_2\text{O}-55\text{Gr})}{k(\text{Cu}-55\text{Gr})}$	$1.390 \pm 0.002$	$0.940 \pm 0.002$	$0.713 \pm 0.001$
$\frac{k(\text{Cu}_2\text{O}-70\text{Gr})}{k(\text{Cu}-70\text{Gr})}$	$1.195 \pm 0.002$	$0.881 \pm 0.001$	$1.218 \pm 0.001$

- At 6 N, the wear rate of the Cu<sub>2</sub>O-70Gr is nearly 40% lower than that of the Cu-70Gr. At 6 N and 10 N, the wear rate of the Cu<sub>2</sub>O-55Gr is nearly 50% lower than that of the Cu-55Gr. More adhesive and abrasion wear of the Cu-Gr composites can be attributed to the relatively bad mechanical properties compared to the Cu<sub>2</sub>O-Gr composites.
- At the load of 2 N, the Cu<sub>2</sub>O-55Gr composite presents a significantly good self-lubrication property in current-carrying friction. The wear rate of the Cu<sub>2</sub>O-55Gr composite is about 25% lower than that of the Cu-55Gr composite. The main wear mechanisms of the composites are adhesive wear and arc ablation.

### ACKNOWLEDGEMENTS

This work was supported by the National Key Research and Development Program of China (2016YFB0301400) and grants from the Project of State Key Laboratory of Powder Metallurgy, Central South University, Changsha, China.

### FUNDING

This work was supported by the National Key Research and Development Program of China (2016YFB0301400) and grants from the Project of State Key Laboratory of Powder Metallurgy, Central South University, Changsha, China.

### CONFLICT OF INTEREST

The authors declare that they have no known competing financial interests or personal relationships that could have appeared to influence the work reported in this paper. On behalf of all authors, the corresponding author states that there is no conflict of interest.

### REFERENCES

- H. Xu, J. Hao Chen, S. Bin Ren, X. Bo He, and X. Hui Qu, *Int. J. Miner. Metall. Mater.* **25**, 459 (2018).
- S.F. Moustafa, S.A. El-Badry, A.M. Sanad, and B. Kieback, *Wear* **253**, 699. (2002).
- S. Ren, J. Chen, X. He, and X. Qu, *Carbon N. Y.* **127**, 412. (2018).
- X.C. Ma, G.Q. He, D.H. He, C.S. Chen, and Z.F. Hu, *Wear* **265**, 1087. (2008).
- T. Futami, M. Ohira, H. Muto, and M. Sakai, *Carbon N. Y.* **47**, 2742. (2009).
- H. Zhongliang, C. Zhenhua, X. Jintong, and D. Guoyun, *Wear* **265**, 336. (2008).
- S. Kang Tang, Z. Li, S. Gong, and Z. Xiao, *J. Cent. South Univ.* **27**, 1158 (2020).
- F. Long, X. Guo, K. Song, J. Liu, X. Wang, Y. Yang, and S. Li, *Compos. Part B Eng.* **229**, 109455. (2021).
- F. Yang, Y. Su, S.Q. Jia, Q.Y. Zhao, L. Bolzoni, T. Li, and M. Qian, *Jom* **71**, 4867. (2019).
- M. Shabani, M.H. Paydar, and M.M. Moshksar, *Int. J. Miner. Metall. Mater.* **21**, 934. (2014).
- Q. Lin, F. Yang, H. Yang, R. Sui, Y. Shi, and J. Wang, *Carbon N. Y.* **159**, 561. (2020).
- L. Wang, J. Li, Z. Che, Xitao, Zhang, Hailong, and Jinguo, *J. Alloy. Compd. An Interdiscip. J. Mater. Sci. Solid State Chem. Phys.* **749**, 1098 (2018).
- Y. Wang, Y. Gao, J. Takahashi, Y. Wan, M. Li, B. Xiao, Y. Zhang, and X. He, *Mater. Chem. Phys.* **239**, 121990. (2020).
- Y. Wang, Y. Gao, J. Takahashi, Y. Wan, B. Xiao, Y. Zhang, X. He, and J. Li, *Vacuum* **168**, 108829. (2019).
- Q. Cui, C. Chen, C. Yu, T. Lu, H. Long, S. Yan, A.A. Volinsky, and J. Hao, *Carbon N. Y.* **161**, 169. (2020).
- W. Zheng, X. Bo He, M. Wu, X. Hui Qu, R. Jun Liu, and D. Dan Guan, *Int. J. Miner. Metall. Mater.* **26**, 1166 (2019).
- Q. Zhang, B. Chen, B. Zhao, S. Liang, and L. Zhuo, *Jom* **71**, 2541. (2019).
- S. Huang, Y. Feng, H. Liu, K. Ding, and G. Qian, *Mater. Sci. Eng. A* **560**, 685. (2013).
- J. F. Li, L. Zhang, J. K. Xiao, and K. C. Zhou, *Trans. Non-ferrous Met. Soc. China (English Ed.)* **25**, 3354 (2015).
- J.H. Nie, C.C. Jia, X. Jia, Y. Li, Y.F. Zhang, and X.B. Liang, *Int. J. Miner. Metall. Mater.* **19**, 446. (2012).
- P.L. Menezes, M. Nosonovsky, S.P. Ingole, S.V. Kailas, and M.R. Lovell, Springer New York, 341 (2013). <https://doi.org/10.1007/978-1-4614-1945-7>.
- B. Liu, D. Zhang, X. Li, Z. He, X. Guo, Z. Liu, and Q. Guo, *J. Alloys Compd.* **766**, 382. (2018).
- J. Kováčik, Š. Emmer, J. Bielek, and L. Keleši, *Wear* **265**, 417. (2008).
- K. Rajkumar, and S. Aravindan, *Tribol. Int.* **57**, 282. (2013).
- Z. Xiao, R. Chen, X. Zhu, Z. Li, G. Xu, Y. Jia, and Y. Zhang, *J. Mater. Eng. Perform.* **29**, 1696. (2020).
- T. Xiang, J. Dai, W. Qiu, M. Wang, Z. Li, Z. Xiao, and Y. Jiang, *Jom* **71**, 2513. (2019).
- J. Chen, S. Ren, X. He, and X. Qu, *Carbon N. Y.* **121**, 25. (2017).
- Q.L. Lin, F. Yang, H.Y. Yang, R. Sui, and J.B. Wang, Wetting of graphite by molten Cu-xSn-yCr ternary alloys at 1373 K. *Carbon* **159**, 561–569 (2020). <https://doi.org/10.1016/j.carbon.2019.12.097>.
- G.C. Yao, Q.S. Mei, J.Y. Li, C.L. Li, Y. Ma, F. Chen, and M. Liu, *Mater. Des.* **110**, 124. (2016).
- C. Wang, and X. Xiangxin, *Dongbei Daxue Xuebao/Journal Northeast. Univ.* **33**, 1290. (2012).
- S.J. Huang, A. Abbas, and B. Ballóková, *J. Mater. Res. Technol.* **8**, 4273. (2019).
- W. Chao, X. Xiangxin, C. Xiaozhou, Y. He, and C. Gongjin, *Arch. Metall. Mater.* **58**, 509. (2013).
- C.P. Samal, J.S. Parihar, and D. Chaira, *J. Alloys Compd.* **569**, 95. (2013).
- H. Sun, N. Deng, J. Li, G. He, and J. Li, *J. Mater. Sci. Technol.* **61**, 93. (2021).
- H. Kurita, T. Miyazaki, A. Kawasaki, Y. Lu, and J.F. Silvain, *Compos. Part A Appl. Sci. Manuf.* **73**, 125. (2015).
- X. Long Liu, Z. Bing Cai, Q. Xiao, M. Xue Shen, W. Bin Yang, and D. Yun Chen, *Int. J. Mech. Sci.* **184**, 105703. (2020).
- W. Ma, and J. Lu, *Tribol. Lett.* **41**, 363. (2011).

38. B. Chen, Q. Bi, J. Yang, Y. Xia, and J. Hao, *Tribol. Int.* 41, 1145. (2008).
39. K. Rajkumar, and S. Aravindan, *Tribol. Lett.* 37, 131. (2010).
40. A. Abbas, S.J. Huang, B. Ballóková, and K. Sülleiová, Tribological effects of carbon nanotubes on magnesium alloy AZ31 and analyzing aging effects on CNTs/AZ31 composites fabricated by stir casting process. *Tribol. Int.* 142, 105982 (2020). <https://doi.org/10.1016/j.triboint.2019.105982>.
41. H. Cao, Z. Qian, L. Zhang, J. Xiao, and K. Zhou, *Tribol. Trans.* 57, 1037. (2014).
42. X.B. Liu, H.Q. Liu, Y.F. Liu, X.M. He, C.F. Sun, M. Di Wang, H.B. Yang, and L.H. Qi, *Compos. Part B Eng.* 53, 347. (2013).
43. Y.A. Wang, J.X. Li, Y. Yan, and L.J. Qiao, *Tribol. Int.* 50, 26. (2012).
44. N.P. Suh, *Wear* 25, 111. (1973).
45. I. L. Singer and H. M. Pollock, *Fundamentals of Friction: Macroscopic and Microscopic Processes* (Fundamentals of Friction: Macroscopic and Microscopic Processes, 1992).
46. V. Hegadekatte, N. Huber, and O. Kraft, *Model. Simul. Mater. Sci. Eng.* 13, 57. (2005).
47. R. Aghababaei, and K. Zhao, *Wear* 476, 203739. (2021).

**Publisher's Note** Springer Nature remains neutral with regard to jurisdictional claims in published maps and institutional affiliations.